JTTEE5 13:570-585
DOI: 10.1361/10599630419391
1059-9630/$19.00 © ASM International

Peer Reviewed

Neural Computation to Predict In-Flight Particle Characteristic Dependences From Processing Parameters in the APS Process

Sofiane Guessasma, Ghislain Montavon, and Christian Coddet

(Submitted February 17, 2003; in revised form May 29, 2003)

In-flight particle sensors for thermal spraying are used for real-time monitoring of coating manufacture. However, such tools do not offer facilities to tune the processing parameters when the monitoring reveals fluctuations or instabilities in the thermal jet. To complete the process control, any diagnostic sensors need to be coupled with a predictive system to separate the effect of each processing parameter on the in-flight particle characteristics. In this work, a nonlinear dynamic system based on an artificial neural network (ANN) model is proposed to play this role. It consists of a method that relates the processing parameters to the particle emitted signal characteristics recorded with a DPV2000 (TECNAR Automation, St-Bruno, QC, Canada) optical sensing device. In such a way, a database was built to train and optimize an ANN structure. The in-flight particle average velocity, temperature, and diameter of an alumina-13wt.%titania feedstock were correlated to the injection and power parameters. Correlations are discussed on the basis of these predictive results.

Keywords artificial neural network, in-flight particle characteristics, optical sensor, processing parameters

1. Introduction

Optical sensors are the most adequate diagnostic tools to monitor the thermal spray process (Ref 1, 2). Developments in this field have permitted recording the two-dimensional (2-D) profiles of in-flight particle characteristics (Ref 3). These characteristics influence both the coating properties (Ref 3-5) and the operating conditions (Ref 3, 6). They constitute, hence, efficient indicators of an "ideal" interface to control the process (Ref 7, 8). Furthermore, the particle-plasma interactions represent the unique stage where on-line control may be operated, since the other stages require off-line analyses. However, diagnostic tools such as the integrated optical monitoring systems diagnose the particle state variations but do not offer opportunities to tune the operation conditions. To do so, the sprayer needs a feedback system requiring at least correlations between each processing parameter and each measured characteristic. These feedback models encounter several difficulties due to the versatility of the process (Ref 9) and the difficulty of decoupling the temperature and velocity effects (Ref 10).

In this work, a model was implemented by considering an application on Al_2O_3-13wt.%TiO_2 clad powder of −53 +15 μm particle size distribution. This powder was sprayed (standoff distance of 125 mm, Sulzer-Metco F4 gun, Wohlen, Switzerland) under various air plasma conditions that mainly influence the in-flight particle characteristics; that is, the power and injection conditions were varied. These conditions considered the following processing parameters: arc current intensity, argon

Sofiane Guessasma, Ghislain Montavon, and **Christian Coddet,** Laboratoire d'Etudes et de Recherches sur les Matériaux, les Procédés et les Surfaces (LERMPS), Université de Technologie de Belfort-Montbéliard (UTBM), Site de Sévenans 90 010 Belfort Cedex France. Contact e-mail: ghislain.montavon@utbm.fr.

List of Symbols

ANN	artificial neural network
MLP	multilayer perceptron
D	average in-flight particle diameter, m
D_{inj}	stand-off distance to the gun centerline axis, mm
E_z	quadratic error between predicted and correct output response
$f[\,]$	activation function or transfer function
$f'[\,]$	first derivative of activation function
I	arc current intensity, A
ID	feedstock injector internal diameter, mm
$I(x_i)$, $O(x_i,y)$	input signal of neuron x_i from layer x
$O(y_i)$	output signal of neuron y_i from layer y
$O(z_k)$	resulted output signal at neuron z_k
P_{net}	net plasma power, W
R^2	correlation factor (−)
r_k	correct output response at neuron k
t	epoch, cycle, or iteration
T	average in-flight particle temperature, °C
V	average in-flight particle velocity, ms
V_{Ar}	argon primary plasma gas flow rate, SLPM
V_{CG}	argon carrier gas flow rate, SLPM
V_{H2}	hydrogen secondary plasma gas flow rate, SLPM
$w(x_i,y_j)$	weight between neuron x_i from the layer x and neuron y_j from the layer y
δ	partial derivation operator
$\underline{\nabla}$	gradient operator

primary plasma gas, hydrogen secondary plasma gas, feedstock carrier gas flow rate, injector standoff distance, and injector internal diameter. The other processing prameters were kept constant to reference values. For each condition, the average particle velocity, temperature, and diameter were recorded at the center of the particle flow stream using an optical sensor (DPV2000, Tecnar, St. Bruno, QC, Canada). A database formed from these experimental sets permitted via a neural network (Fig. 1) each of the considered processing parameters to be related to each of the particle characteristics.

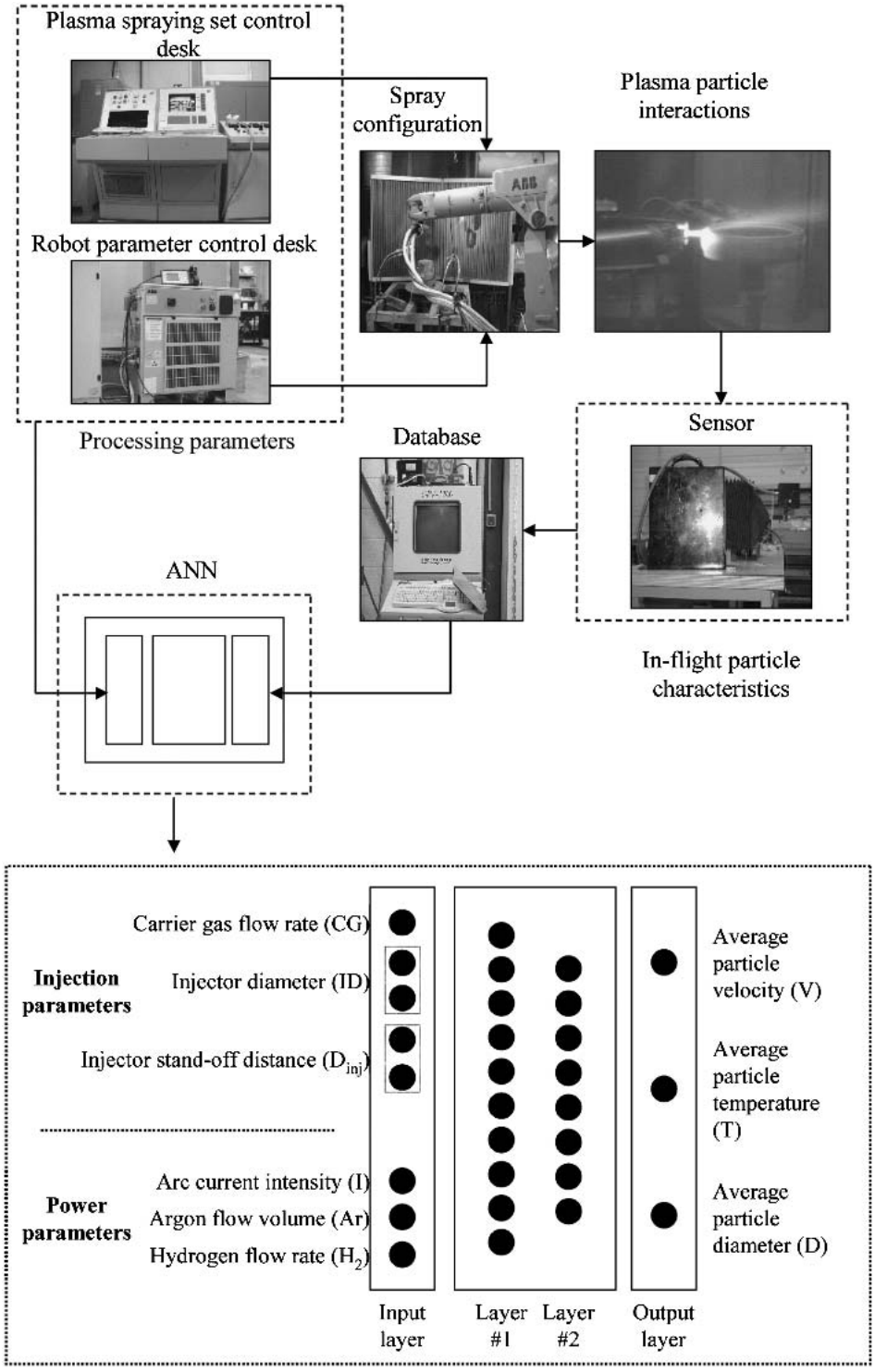

Fig. 1 ANN implementation in the APS process

2. In-Flight Particle Characteristics Measurement

Most open, close, and feedback control systems use sensors to monitor fluctuations in the plasma jet and measure their direct effects on the in-flight particle characteristics (Ref 3, 11). Several methods are implemented to measure the particle velocity, temperature, and diameter, such as pyrometry, particle image velocimetry (PIV), and particle shape image (PSI) techniques (Ref 3, 11, 12). The DPV2000 system is one of the most popular devices based on pyrometric analysis and was used in this study to monitor the spray process. In this system, a sensing head ensures the collection of the particle characteristics. It is mounted on a computer-aided displacement device allowing radial displacements at a given spray distance. This sensor collects thermal radiations of particles (i.e., approximated as gray bodies) as they pass in the measurement volume of about 0.1 mm^3 (Ref 3). A dual-response signal is detected by a photo mask and allows the calculation of three parameters.

The particle velocity is calculated by dividing the distance between the images of the two photo mask slits in the measurement volume by the time of flight between the two responses. The measurement range is from 30 to 1200 m/s, depending on the selected photo mask. The particle temperature is determined by considering the ratio of the signals (i.e., radiance) recorded by two wavelength detectors. The typical range is from 1000 to 4000 °C. The gray body theory and constant emissivity are assumed for all particles. Finally, the particle diameter can be established considering either the proportionality to the particle response signal or the time integral of the complete signal. The typical range of measurement is between 10 and 300 μm. A calibration procedure is required to correct the diameter coefficient due to the emissivity sensitivity to the material nature and spray conditions. This calibration can be expressed as:

$$\text{new coefficient} = \text{original coefficient} \times \left(\frac{\text{average in-flight particle diameter}}{\text{average powder size distribution}}\right) \quad \text{(Eq 1)}$$

An auto centering routine was considered to record the in-flight particle characteristics at the maximum of the particle flow. Thus, the *y* position varied from one condition to another, varying from 4 to 13 mm apart from the gun centerline axis.

3. Simulation Model

3.1 Artificial Neural Networks

Previous studies demonstrated the applicability of fuzzy logic and artificial intelligence concepts to thermal spray process modeling (Ref 13, 14). The artificial neural network (ANN) model belongs to dynamic system models, which are applied to recognize physical properties and optimize manufacturing processes. In addition, it offers wide possibilities of dynamic controlling, that is, determining which action must be taken to reproduce expected coating in-service properties. The process modeling principle is presented hereafter, and its mathematical basis is given in Appendix 1.

The ANN model is based on the discrimination of complex correlations between the process input (I) and the process output (O) in a large, but simple, mathematical operation processed through units called neurons. These processing elements act as decision cells "feeding" the results of the "within operations" to the other neurons by means of connections. The strength of a given connection is quantified by a number, which is termed as a weight. An optimized neuron structure considers the adequate weight population that best describes the I/O correlations (Fig. 2). This population is discovered by a training procedure to learn the I/O examples from experimental sets. The way the weights are tuned is called a paradigm (Appendix 1). The most popular and powerful paradigm used to train ANN is the back propagation paradigm (Ref 15-17) developed between 1974 and 1985. This paradigm needs multiple I/O examples to achieve the ANN structure optimization (i.e., the adequate network setup parameters, the smallest neuron number and the optimal neuron population). The paradigm used in this study is a "faster" variation of standard back propagation (Ref 17) (Appendix 1), also called "quick" back propagation.

3.2 Model Implementation

Before implementing any model dealing with process control, special care is needed in selecting the I/O categories. In the case of the thermal spray process, several authors reported a subdivision of the process based on chronological events occurring during the process (Ref 1, 18-20) with the evidence being that each stage of the process deals with different I/O categories (Ref 20). For example, Moreau (Ref 1) reported three major zones: heat generation, particle heating and acceleration, and coating buildup. These studies agree in considering the prevailing role of in-flight particle characteristics as an efficient indicator of the parameter stabilities (Ref 21). Furthermore, these characteristics proved to directly influence the coating microstructure and the physical-mechanical properties (Ref 4). In the following model, these characteristics; namely average velocity, temperature, and diameter—are considered as the output units (Table 1). From this set of output units, the particle flow rate was not considered and it was kept constant. Each of these characteristics is labeled with one neuron since they constitute real variables.

The adequate conversions (which are also valid for the input parameters) are taken into account to set each input between 0 and 1:

$$x = \frac{x - x_{\min}}{x_{\max} - x_{\min}} \quad \text{(Eq 2)}$$

where x is a real value of an input or output unit and $x_{\min}$ and $x_{\max}$ are the limits of each x unit determined from the physical limitations of the process and not from the maximum and minimum values of the experimental sets.

This set of particle characteristics is mainly influenced by two categories of processing parameters, namely the power and the feedstock injection parameters. The particle drag coefficient,

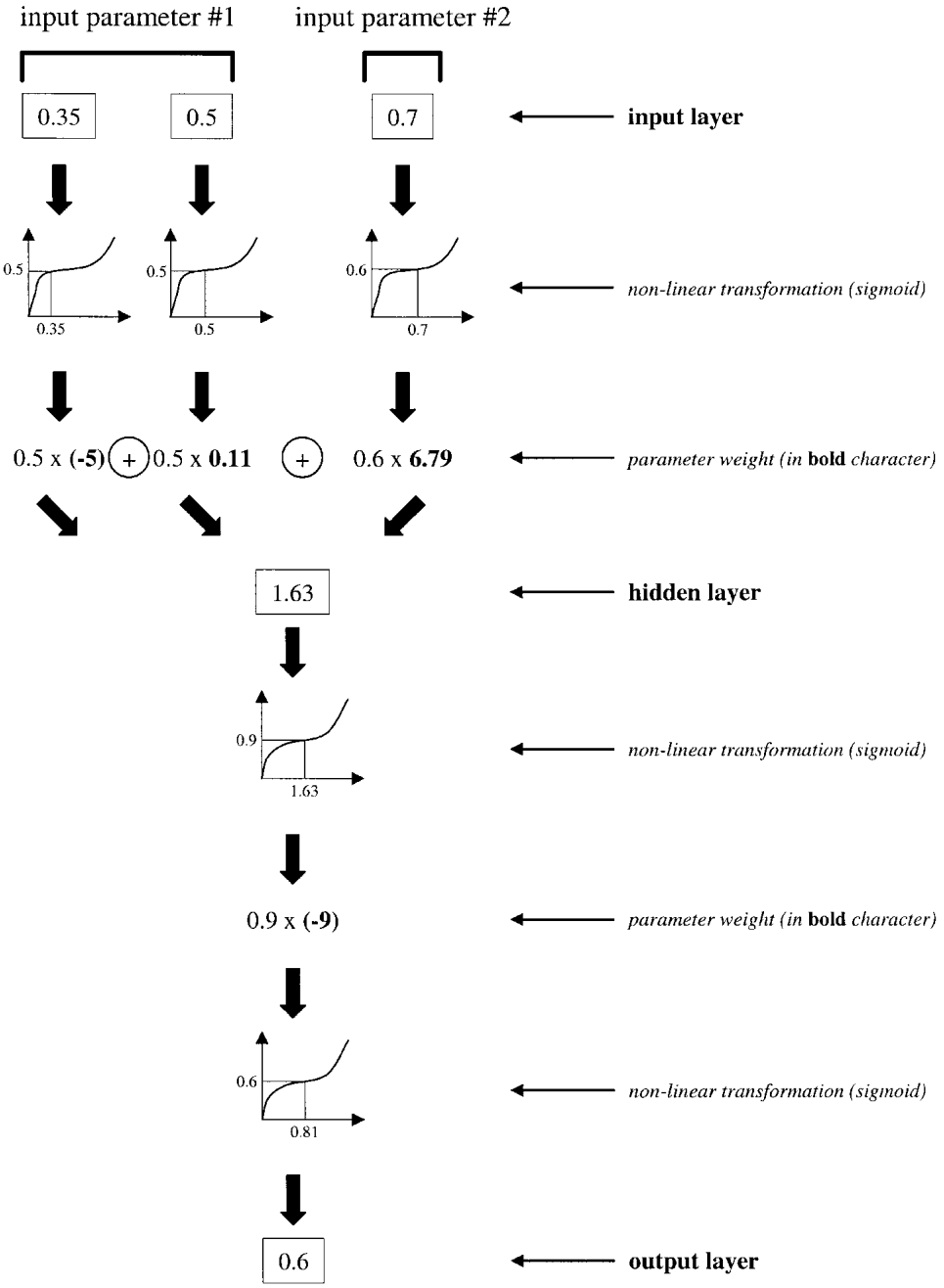

Fig. 2 Connective scheme of a simple ANN

the amount of heat transfer, and the acceleration depend on the plasma jet properties (i.e., gas density, velocity, thermal conductivity, etc.) (Ref 22, 23). These latter properties are directly related to the arc-gas properties and the torch design (Ref 24). In addition, powder and powder-feed variables highly influence the particle trajectory and their residence time in the jet (Ref 7). As previously mentioned, the selected processing parameters belonging to the considered categories were the current intensity (I), the argon primary gas flow rate (V_{Ar}), the hydrogen secondary gas flow rate (V_{H2}), the carrier gas flow rate (V_{CG}), the injector standoff distance (D_{inj}), and the injector internal diameter (ID). One neuron described the real values of I, V_{Ar}, V_{H2}, and V_{CG} parameters, whereas a classification appeared to be necessary to deal with the values related to D_{inj} and ID. In fact, it is not possible to vary these parameters continuously. Thus, they are considered as categories to be selected. The ANN methodology allows such description requirement: x neurons for 2^x categories (Fig. 1).

Table 1 summarizes the selected parameters used as input and output units for this study.

Based on these selected parameters, a simple multilayer perceptron (MLP) was built considering a feed forward architecture (see Appendix, Fig. A1). Several studies have described the rela-

Table 1 ANN variables. Parameter values in bold type refer to the reference condition.

Layer	Variable	Symbol	Value	Number of neurons
Input	Arc current intensity, A	I	350, **530,** 750	1
	Argon gas flow volume, SLPM	V_{Ar}	(40,0)(a), (40,4), (40,8), (40,8), (40,10)	1
	Hydrogen flow volume, SLPM	V_{H2}	**(40,14),** (22.5,7.5), (37.5,12.5)	1
	Carrier gas flow rate, SLPM	V_{CG}	2.2, **3.2,** 4.4	1
	Injector diameter, mm	ID	1.5, **1.8,** 2.0	2
	Injector standoff distance, mm	D_{inj}	**6,** 7, 8	2
Output	Average particle velocity, m/s	V	…	1
	Average particle temperature, °C	T	…	1
	Average particle diameter, μm	D	…	1

(a) (V_{Ar}, V_{H2})

Table 2 Neural network setup and the related parameters

Category	Parameter	Description	Optimized values
Architecture		Connection scheme between neurons	Normal feed-forward (suitable for most applications)
Layer definition	Hidden layer number	Number of neuron layers between I/O categories	2 (value required for non-linear systems)
	Learning rule (a)	Paradigm used to tune the weight values in each hidden layer and output layer	Quick propagation (a fast variation of standard back propagation)
	Number of neurons	Nodes required to relate the I/O categories	10 in the first layer and 8 in the second layer (obtained at the end of the optimization process)
	Input function	Statement of how the result of a layer feed a given neuron. It concerns the hidden and output layers	Dot product between neuron outputs
	Input preprocessing	Data conversion if applicable. It concerns only the input layer	None
	Transfer function	Nonlinear conversion of the neuron outputs sum	Sigmoid (most suitable since it compresses the neuron input when large weight negative of positive values are reached)
Network error type		Energy of the optimization process	Mean absolute error between calculated and experimental outputs (mostly recommended)
Training and testing	Batch size	Determination of the number of samples processed before the weight update	1
	Input set	Determination of either single test or training pass to be tested	Training set as input
	Maximum iterations	First of the stopping criteria. This fixes the number of weight updates	920
	Tolerance	Second cumulative criterion with the cycle number	0.001 (it was not reached)
	Sequencing	Determination of the order of training and testing	Training + test pass before weight update

(a) Dependent on the network architecture

tive simplicity of the neural networks required to process such problems (Ref 25, 26). The choice of the network architecture is justified by the nature of the correlations that have to be discovered. Roughly speaking, these correlations can be considered for this application as a problem of function approximation in the parameter space. Consequently, the feed forward architecture seems to be the most suitable scheme (Ref 27).

Before optimizing the considered ANN system, prior knowledge of the nature of the correlations has to be considered to fix the required layers between the I/O categories. For the case of a linear system, generally one layer is sufficient. In the case of thermal spray process, these correlations are mostly nonlinear (Ref 4), and two layers are required.

3.3 ANN Optimization Process

The ANN optimization process was already presented in a previous study (Ref 28). Here is a brief description of the required steps.

Step one consists of building the database. It takes into account the physical limits of each process parameter (i.e., a maximum plasma gas flow rate for example) and the trivial situations where no generation of plasma (arc current intensity equal to zero for example) or material feed (a carrier gas flow rate equal to zero for example) is possible. However, experimental sets are required to train the neural net to recognize the physical correlations. The parameters were varied individually from reference conditions to the limits values (Table 1).

In a second step, a network is set up. This is described by several parameters listed in Table 2. Each parameter was adapted to meet the requirements of the study; the optimization of such parameters was undertaken considering a part of the database, which is named the validation category. A previous study presented different configurations for each parameter and the related results (Ref 28).

Training and test procedures are performed in step three. This is an essential step of the optimization process. Both training and test procedures are processed with different I/O examples re-

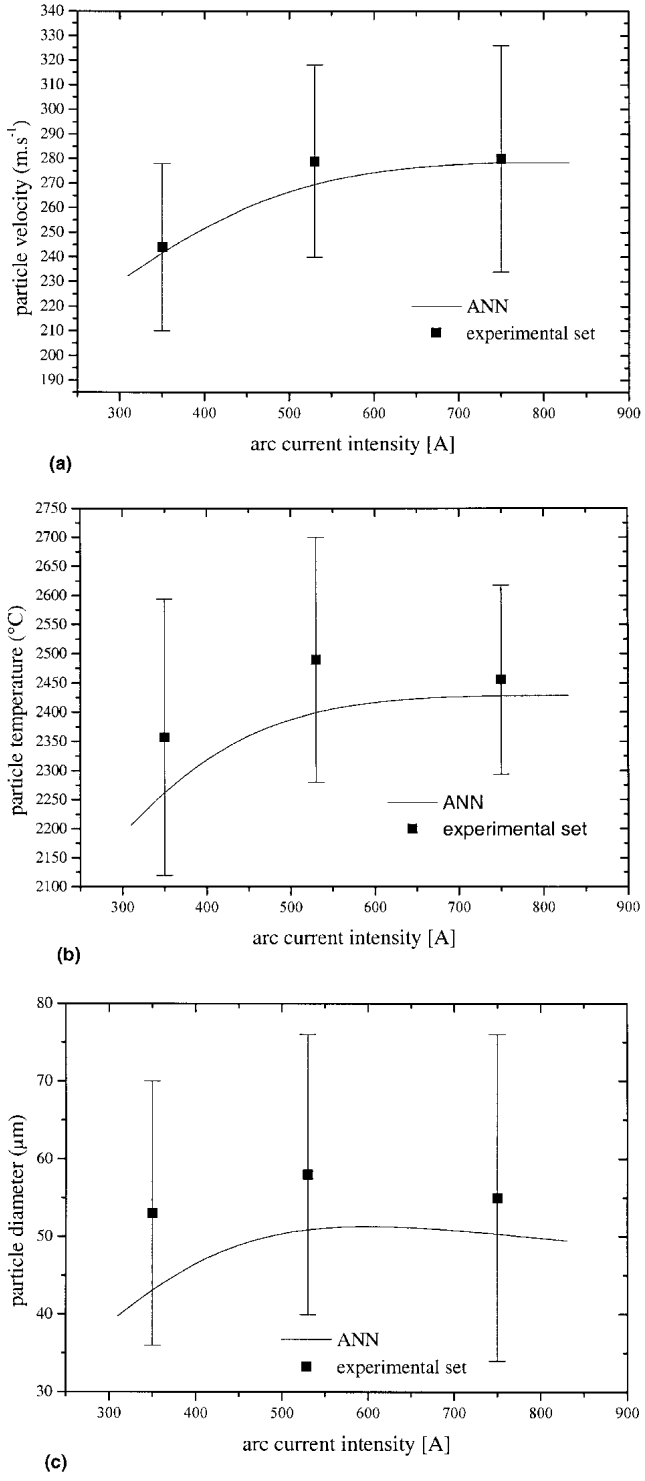

Fig. 3 Predicted particle (a) velocity, (b) temperature, and (c) diameter as a function of the arc current intensity

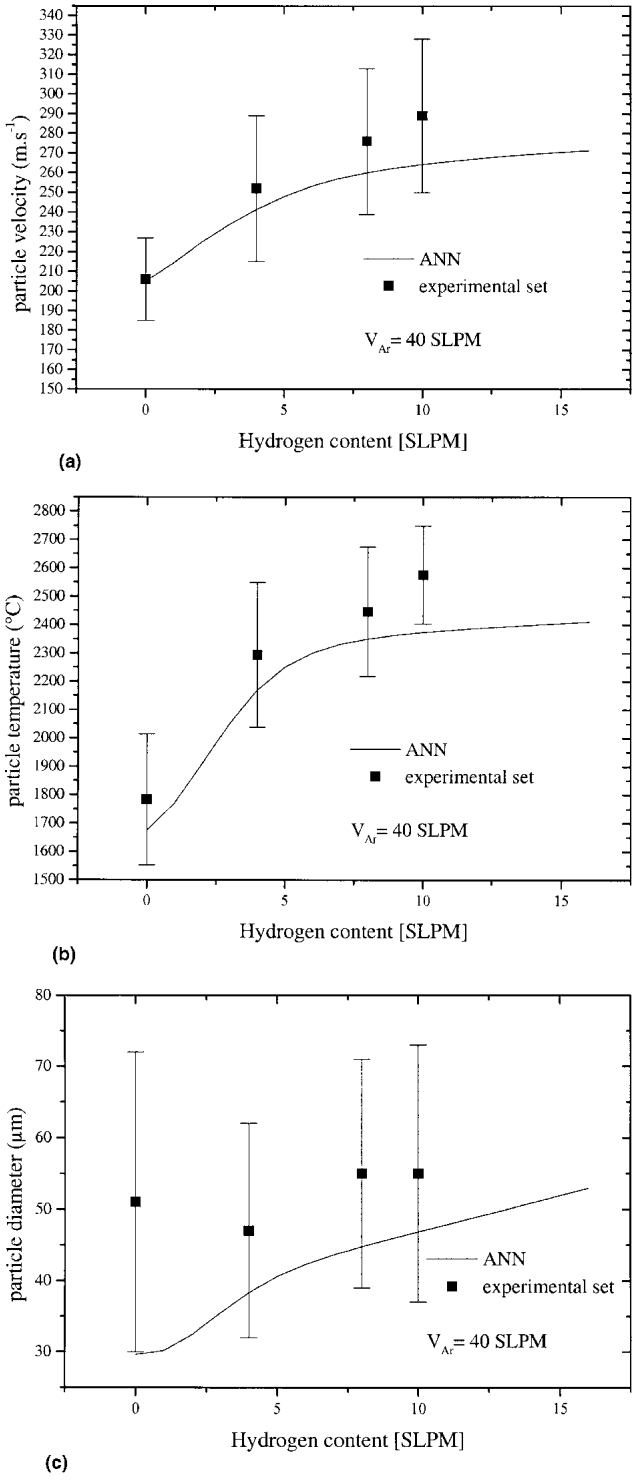

Fig. 4 Predicted particle (a) velocity, (b) temperature, and (c) diameter as a function of the hydrogen content

quiring a subdivision of the database into training and test categories, respectively.

The final step is the generalization procedure. It assumes that the results of the validation, training, and test procedures permit generalization of the results of the studied correlations. In a first step the experimental and predicted values are compared. Then, correlations are extrapolated for intermediate processing parameter values. Figures 3 to 6 present these correlations.

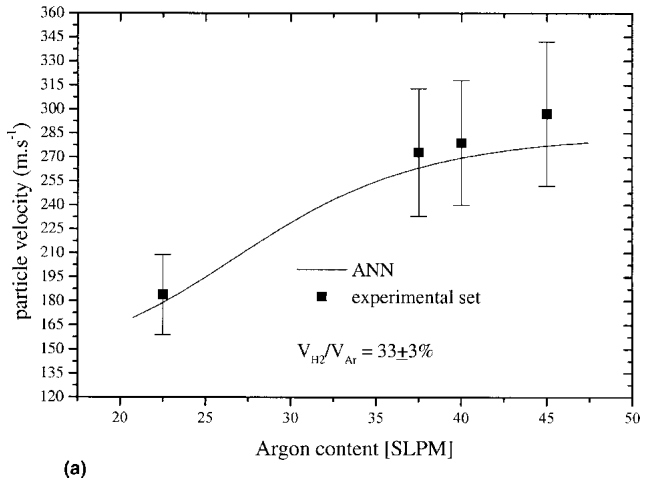

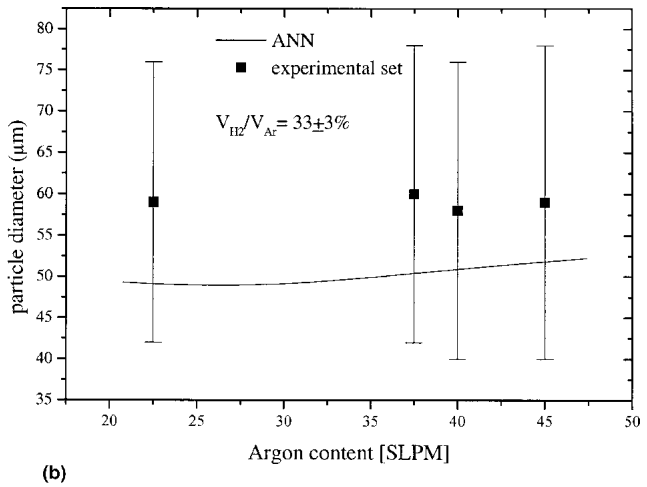

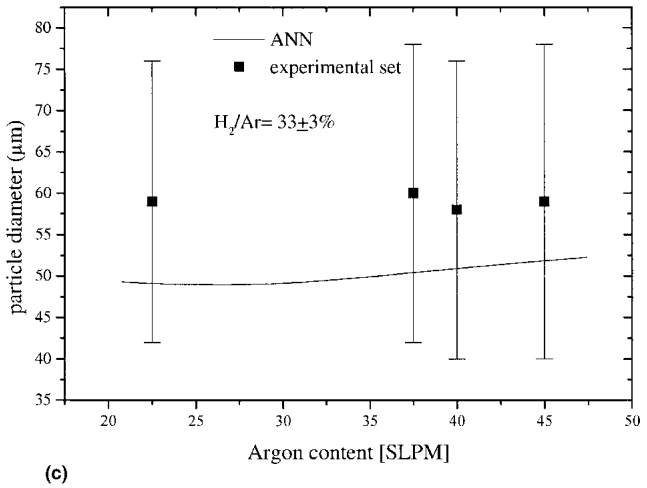

Fig. 5 Predicted particle (a) velocity, (b) temperature, and (c) diameter as a function of the argon content

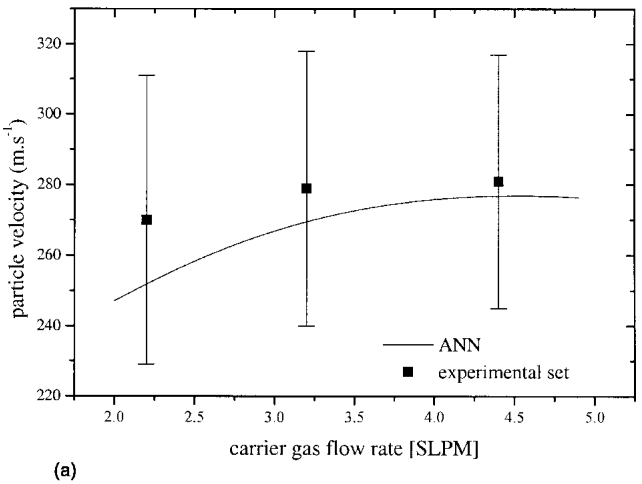

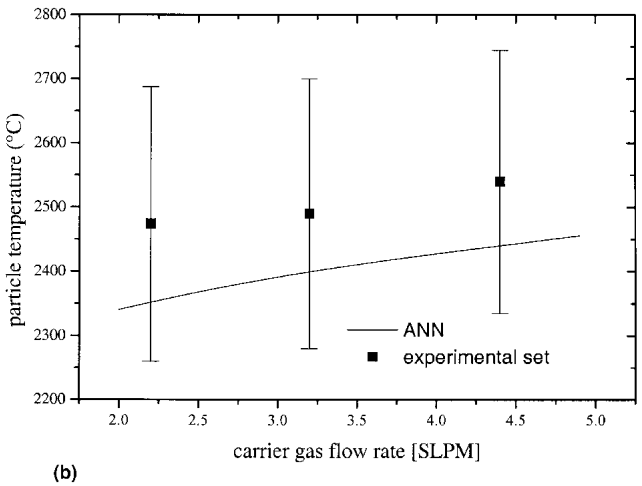

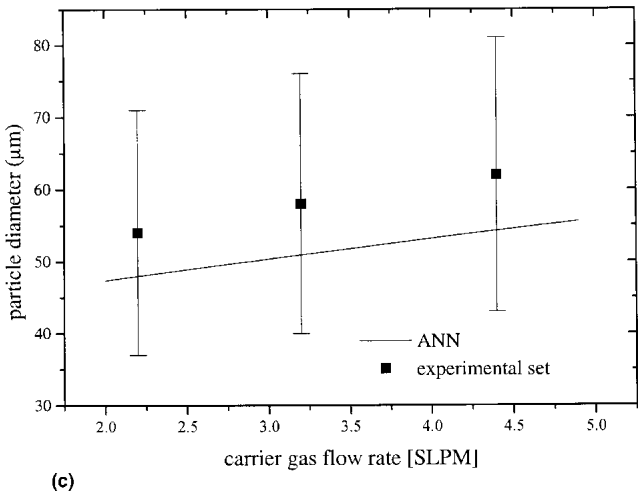

Fig. 6 Predicted particle (a) velocity, (b) temperature, and (c) diameter as a function of the carrier gas flow rate

4. Results and Discussion

4.1 Preliminary Analysis

Experimental in-flight particle characteristics obtained with the DPV2000 sensor at the center of the particle flow stream exhibit a relatively high scatter, especially concerning the diameter measurements. From this point of view, the standard deviations are 37 m/s (14% of the average value), 205 °C (8% of the average value), and 18 µm (32% of the average value), respec-

tively for V, T, and D. Leblanc et al. (Ref 8) reported variations of the same magnitudes of about 200 °C and 30 m s^{-1} on temperature and velocity during 45 h of spraying in the case of a zirconia powder having a comparable size distribution (i.e., −45 +22.5 μm). This scatter was essentially attributed in that case to electrode wear. After 68 h of spraying at the time of measuring, the net power exhibited strong fluctuations with the consequence of increasing the cold particle fraction in the plasma jet (Ref 7, 9). In the current study, the mean values give, however, a satisfactory tendency comparable to the results of the predicted curves.

The predicted curves are the results of the whole database treatment. Thus, they do not represent actually fitting procedure results but rather correlation sets. To generalize the proposed network structure, at least three experimental points for each condition were compared with the predicted tendencies.

Figures 3 to 6 show the effects of the studied parameters on V, T, and D characteristics. Generally speaking, the results point out, particularly, the very significant effects of V_{Ar} and V_{H2} on V and T for the studied conditions. Guilemany et al. (Ref 5) found the same effects in the case of a stainless steel powder. The D characteristic results are more difficult to analyze. The mean diameter was found for most cases to be outside the considered distribution range. This result arises mainly because the high scatter of the experiments produced no meaningful variations on D. However, some correlations were reported on the D variations, especially those resulting from models showing that generally D decreases with an increase of T and V characteristics (Ref 10, 29).

Correlations discovered by ANNs result from a compromise between the representativeness of the data points in the process parameter space and the learning criteria. This is the reason why the predicted correlations presented in Fig. 3-6 lay below, in these specific cases, the experimental validation points. Of course, closer data points would permit a better local description of a given correlation, but its generalization to the whole process parameter space is not possible anymore, reducing in such a way the interest of implementing such a methodology.

4.2 Influence of the Arc Current Intensity on Particle Characteristics

Figure 3 shows the predicted evolutions of the average particle velocity, temperature, and diameter as a function of the arc current intensity.

Parameters T and V exhibit a parabolic increasing dependence with the arc current intensity. Variable D shows the same dependence, but with a slight decrease for high current values. Linear dependences were reported between V and T characteristics (Ref 7) and between each of V and T characteristics considering the net or the effective power (Ref 28, 30).

These results demonstrate quantitatively the effect of the electrical input power in producing optimal particle melting. The improvement of the in-flight characteristics with increasing electric power was also reported by several authors for different materials (Ref 1, 7, 10, 31, 32).

In the case of the studied conditions, the predicted results showed the following relationships:

$$T(°C) = 12 \times 10^{-3} P_{net}(W) + 2101;\ R^2 = 0.95* \quad \text{(Eq 3)}$$

$$V(m/s) = 2.6 \times 10^{-3} P_{net}(W) + 206;\ R^2 = 0.97 \quad \text{(Eq 4)}$$

$$T(°C) = 4.61 \times V(m/s) + 1152;\ R^2 = 0.99 \quad \text{(Eq 5)}$$

$$V(m/s) = 4.23 \times 10^{+6} D(\mu m) + 60;\ R^2 = 0.92 \quad \text{(Eq 6)}$$

It is pointed out that in Eq 6, D represents the mean diameter of particle. Thus, this correlation does not represent the result of an aerodynamic drag model (Ref 10) but the effect of the size distribution shift.

The relatively low correlation factor in Eq 6 is due to the decrease of particle diameter for high arc intensity values, as shown in Fig. 3(c).

4.3 Influence of the Hydrogen Content on Particle Characteristics

Figure 4 shows the predicted evolutions of the average particle velocity, temperature, and diameter as a function of the hydrogen content (V_{H2}).

As for the case of the current, these curves show an increase of the characteristics with an increase of V_{H2}. It is well known that hydrogen improves the velocity, temperature, and enthalpy of the plasma jet (Ref 33) and so the heat and momentum transfer to particles (Ref 34). These, in turn, improve the characteristics (Ref 19, 20, 32).

In the case of the studied conditions, the predicted results showed the below relationships:

$$T(°C) = 50.5 \times 10^{-3} P_{net}(W) + 1396;\ R^2 = 0.99 \quad \text{(Eq 7)}$$

$$V(m/s) = 4.2 \times 10^{-3} P_{net}(W) + 181;\ R^2 = 0.98 \quad \text{(Eq 8)}$$

$$T(°C) = 11.96 \times V(m/s) - 760;\ R^2 = 0.99 \quad \text{(Eq 9)}$$

$$V(m/s) = 3.45 \times 10^{+6} D(\mu m) + 105;\ R^2 = 0.99 \quad \text{(Eq 10)}$$

One has to note that, from a general point of view, these results better fit the assumed linear relationships compared with the I parameter.

4.4 Influence of the Argon Content on Particle Characteristics

Figure 5 shows the predicted evolutions of the average particle velocity, temperature, and diameter as a function of the argon content.

Increasing the argon flow rate (V_{Ar}) increases the particle velocity but decreases the temperature. This result is qualitatively

*R^2 represents the coefficient of multiple determinations, or correlation factor. It calculates the percentage of the data points that could be explained by the relationship. $R^2 = 1$ means that all points are described exactly by the interpolation curve; i.e., every experimental point would lie on the calculated curve.

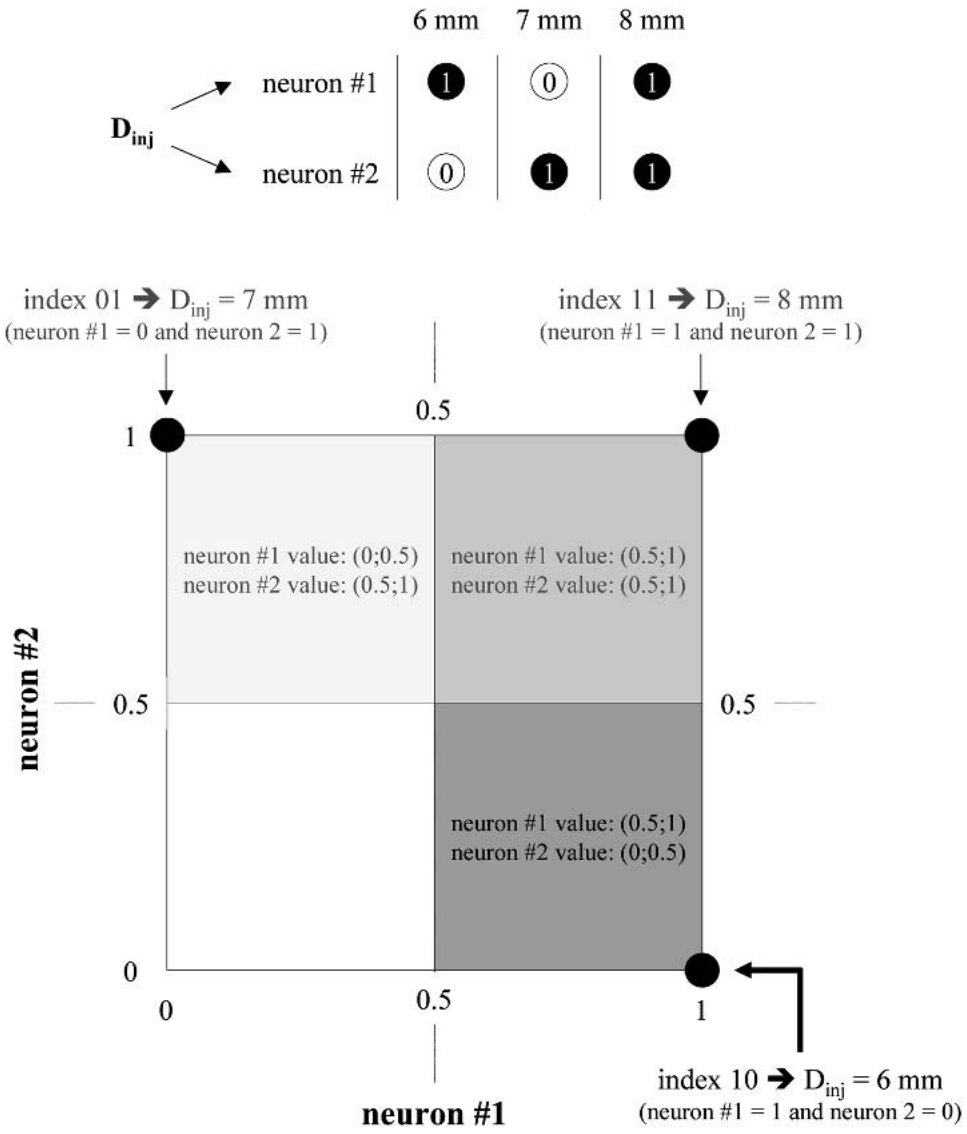

Fig. 7 Neuron attributes for classification: case of the injector stand-off distance (D_{inj})

Table 3 *V, T,* and *D* average values derived from the surface decision of the D_{inj} and ID neurons used to classify each of the considered categories

Input				Output		
Parameter		Neuron #1	Neuron #2	*V*, m/s	*T*, °C	*D*, µm
D_{inj}, mm	6	1	0	297 ± 16	2521 ± 70	60 ± 6
	7	1	1	283 ± 13	2487 ± 28	53 ± 2
	8	0	0	299 ± 17	2543 ± 78	61 ± 7
ID, mm	1.5	0	0	291 ± 18	2577 ± 82	53 ± 2
	1.8	1	0	298 ± 19	2571 ± 99	53 ± 5
	2.0	1	1	292 ± 25	2446 ± 220	45 ± 4

in agreement with previous works (Ref 10, 31, 32) and is directly related to an increase of the momentum transmitted from the plasma jet to the particles, leading to a decrease of their residence time in the hot core of the jet.

The predicted *V* results show a parabolic relationship, whereas a linear dependence of *V* with V_{Ar} parameter was reported in Ref 30.

It seems that *D* is not significantly influenced by the V_{Ar} parameter.

In the case of the studied conditions, the predicted results show the following relationships. The point corresponding to V_{Ar} = 22.7 SLPM and V_{H2} = 7.5 SLPM was not considered because it exhibited singular values due to spray conditions apart from "regular" spray conditions; that is, the gun was operated at the margin of its capabilities.

$$T(°C) = -3 \times 10^{-6} P_{net}{}^2(W) + 119 \times 10^{-3} P_{net}(W) + 1109;\ R^2 = 1 \quad \text{(Eq 11)}$$

$$V(m/s) = -4 \times 10^{-6} P_{net}{}^2(W) + 175 \times 10^{-3} P_{net}(W) - 1628;\ R^2 = 1 \quad \text{(Eq 12)}$$

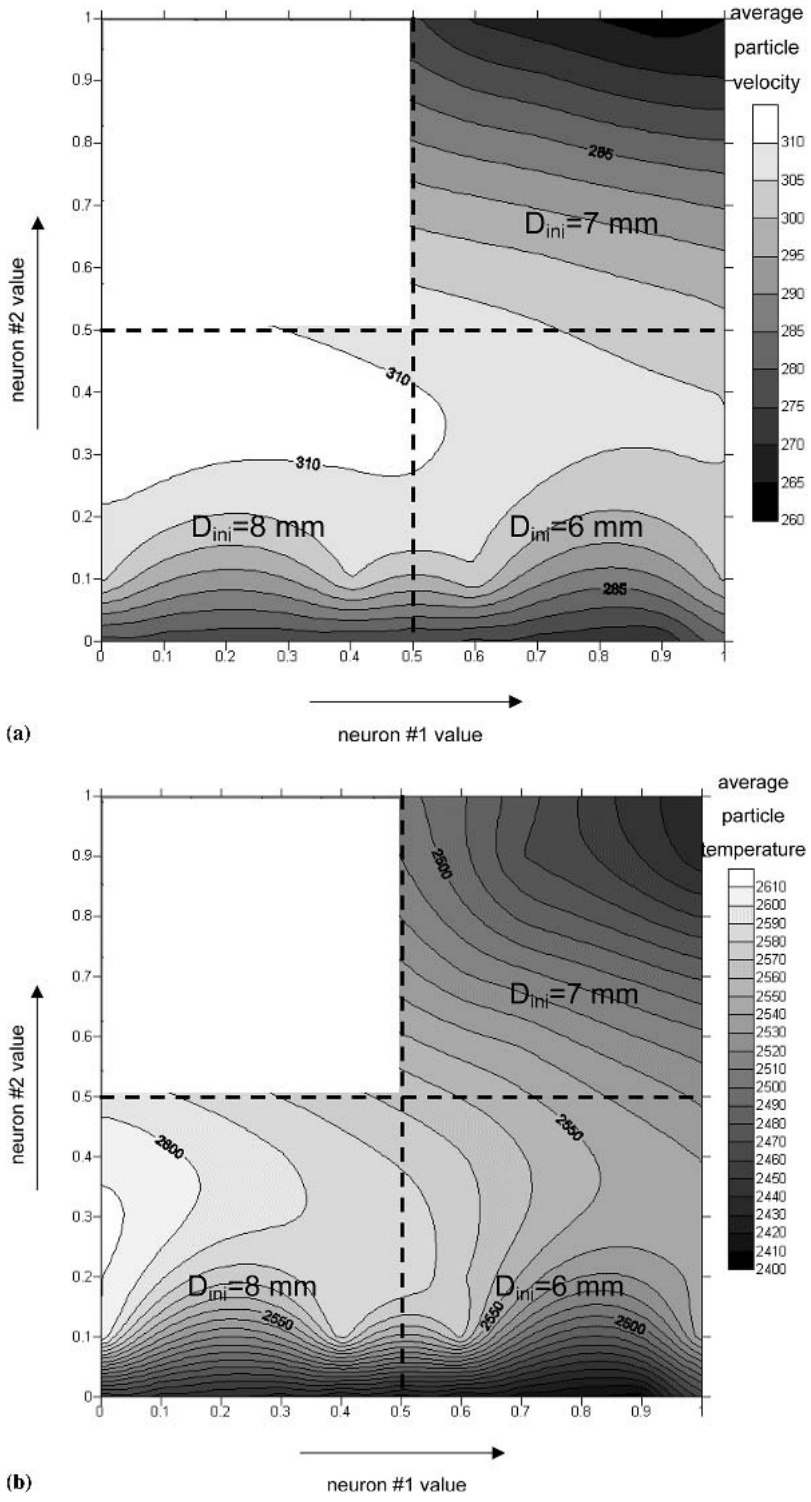

Fig. 8 Contour map of the D_{inj} input unit values showing the dispersion of the (a) V, (b) T. (Continued on next page)

$$T(^{\circ}\mathrm{C}) = 0.015 \times V^2(\mathrm{m/s}) - 7.24 \times V(\mathrm{m/s}) + 3290;\ R^2 = 1 \quad \text{(Eq 13)}$$

$$V(\mathrm{m/s}) = -21 \times 10^{+12} D^2(\mu\mathrm{m}) + 2153 \times 10^{+6} D(\mu\mathrm{m}) - 54{,}959;\ R^2 = 0.99 \quad \text{(Eq 14)}$$

4.5 Influence of the Carrier Gas Flow Rate on Particle Characteristics

Figure 6 shows the predicted evolutions of the average particle velocity, temperature, and diameter as a function of the carrier gas flow rate (V_{CG}).

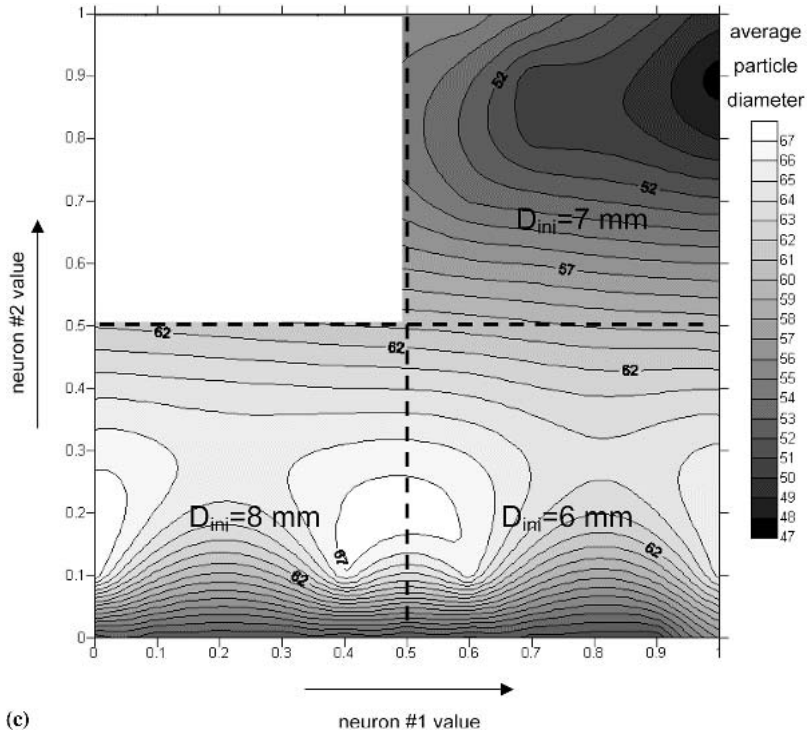

Fig. 8 cont. Contour map of the D_{inj} input unit values showing the dispersion of the (c) *D* results through the domains of the considered categories (6, 7, and 8 mm)

The predicted results show that *V* and *T* increase with an increase of V_{CG}. The same effects were reported by Döring et al. (Ref 10) for yttria stabilized zirconia, in the case, however, of a lower carrier gas flow rate range. The *V*, *T*, and *D* evolutions show a continuous increasing effect, compared for example to the previous parameters (i.e., *I*, V_{Ar}, and V_{H2}). For *V* and *T*, it seems very likely that the optimal injection conditions are higher than the considered range. In the case of the studied conditions, the predicted results showed the correlations:

$$T(°C) = 3.2 \times V(m/s) + 1545; R^2 = 0.98 \quad \text{(Eq 15)}$$

$$V(m/s) = 4.32 \times 10^{+6} D(\mu m) + 46; R^2 = 0.95 \quad \text{(Eq 16)}$$

4.6 Influence of the Injector Standoff Distance on Particle Characteristics

To deal with the results of the classification provided by the optimized network structure for each considered injector diameter, the inputs of the injector standoff distance were varied in the limits of their domain. The decision surface separating each category could be drawn from these variations. For example, in the case of the injector standoff distance of 6 mm indexed by 10 (i.e., neuron No. 1 = 1 and neuron No. 2 = 0), the first neuron value was varied in the range (0.5-1) and the second one in the range (0-0.5) (Fig. 7). These values fed the optimized network structure and the outputs were then averaged. Figure 8 shows the distribution of the *V*, *T*, and *D* values for several input values. Table 3 shows the predicted mean particle velocity, temperature and diameter and the corresponding standard deviations, as a function of the D_{inj} parameter.

Counter plots show qualitatively that *V*, *T*, and *D* increase in the same direction at most of the input values. This is confirmed by the average values displayed in Table 3.

With D_{inj} equal to 7 mm, *V*, *T*, and *D* were the lowest determined values. These results are controversial since the effect of D_{inj} may produce a monotonous variation of *V* and *T* parameters: *V* and *T* increase when D_{inj} decreases (i.e., when the injector tip is closer is closer to the jet core) and inversely. However, the average values are close in the range that states on the favor of a minor effect, for the reference condition at least.

In the case of the studied conditions, the predicted results showed the following correlations:

$$T(°C) = 3.1 \times V(m/s) + 1612; R^2 = 0.92 \quad \text{(Eq 17)}$$

$$V(m/s) = 1.96 \times 10^{+6} D(\mu m) + 180; R^2 = 1 \quad \text{(Eq 18)}$$

In the case of the *T*-*V* correlation, a second-order polynomial function furnished a better approximation.

4.7 Influence of the Injector Diameter on Particle Characteristics

As in the case of the D_{inj} parameter, the same analysis for the injector diameter (ID) was assumed; that is, for each category of injector standoff distance, the inputs of the injector diameter were varied in the limits of their domain. The classification of the three studied categories permitted calculation of the surface contours of the *V*, *T*, and *D* distributions as a function of the input at neuron No. 1 and neuron No. 2 (Fig. 9). Table 3 summarizes the average values obtained for each category.

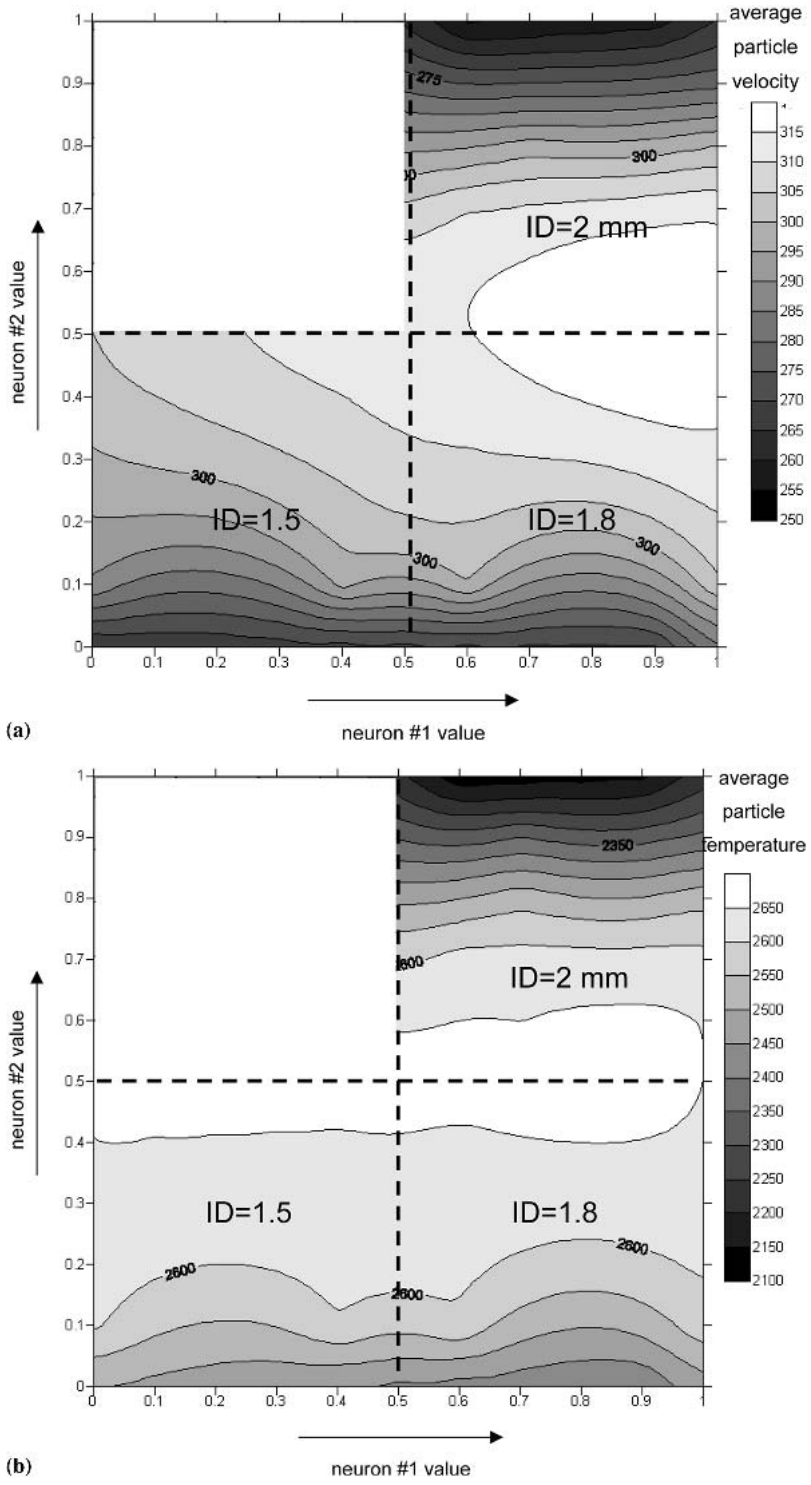

Fig. 9 Contour map of the ID input unit values showing the dispersion of the (a) V, (b) T

The counter plots show the same correlations as in the case of the parameter D_{inj}: a significant coupled effect between V and T and a lower dependence with D. However, average values are not conclusive, first due to the high scatter in the experimental examples and second due to the low scatter in the predicted results. The latter showed an optimal working point at ID = 1.8 mm. In fact, an increase of ID should be very likely accompanied by a decrease of the injection velocity, which in turn can modify V and T, depending on the position of the particles in the plasma jet.

In the case of the studied conditions, the predicted results showed the following correlations:

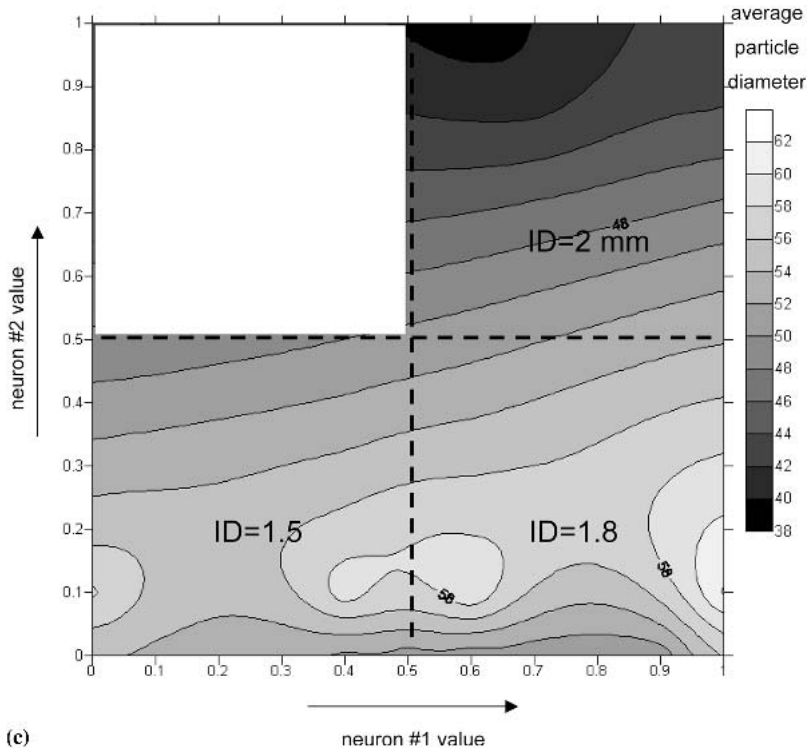

Fig. 9 cont. Contour map of the ID input unit values showing the dispersion of the (c) *D* results through the domains of the considered categories (1.5, 1.8, and 2.0 mm)

$$T(°C) = 26 \times V^2(m/s) - 15{,}086 \times V(m/s) + 2 \times 10^6; \quad R^2 = 1 \qquad \text{(Eq 19)}$$

$$V(m/s) = -1.86 \times 10^{+12} D^2(\mu m) + 182 \times 10^{+6} D(\mu m) - 4151; \; R^2 = 1 \qquad \text{(Eq 20)}$$

5. Conclusions

An ANN model was implemented to study the relationships between some injection/power processing parameters and in-flight particle characteristics. This model required a database obtained with experiments that used the DPV2000 sensor.

High scatter on *V*, *T*, and *D* characterized the measurements due to the experimental conditions. The *D* results were not so discriminative due to the narrow size distribution of the powder used in this study.

A global behavior based on the sampling of the space parameter correlations permitted decoupling the effect of each parameter and relating them with representative curves for each the particle characteristic.

Major effects were discriminated, especially those related to power parameters. The ANN architecture predicted, for example, the *V-T* dependence for each specific case. These effects qualitatively agree with results implementing design of experiment methods reported by several authors (Ref 32, 35, 36). However, the nonlinearity of the correlations is more pronounced in the case of ANN methodology.

The most controversial predicted results are relative to the ID and D_{inj} parameters. In fact, the classification into categories, which was assumed to represent each parameter value, seems to be suitable, but the network setup did not consider specific parameters for such units (such as, for example, the input preprocessing, the activation function, etc.). It is believed that a more adaptive parameter would allow better results.

ANN seems to be a suitable tool to be incorporated in an online control system coupled with a diagnostic tool. A robust database can be used to implement the basis of the control. As the decoupled correlations are recognized for each processing parameter in the ANN structure, it is easier to anticipate for such a system the appropriate combinations to correct parameter aberrations. Therefore, an associated automaton can decide which of the equivalent solutions is the best one guaranteeing the process stability.

Acknowledgment

The authors gratefully thank Patrick Gougeon (LERMPS-UTBM) for his valuable help during the diagnostic experiments. LERMPS is a member of the Institut des Traitements de Surface de Franche-Comté (ITSFC, Surface Treatments Institute of Franche-Comté), France.

Appendix

A1. Mathematical Background of Feed Forward Neural Networks

Following the illustration given in Fig. A1 and A2, the input to a processing element is given by:

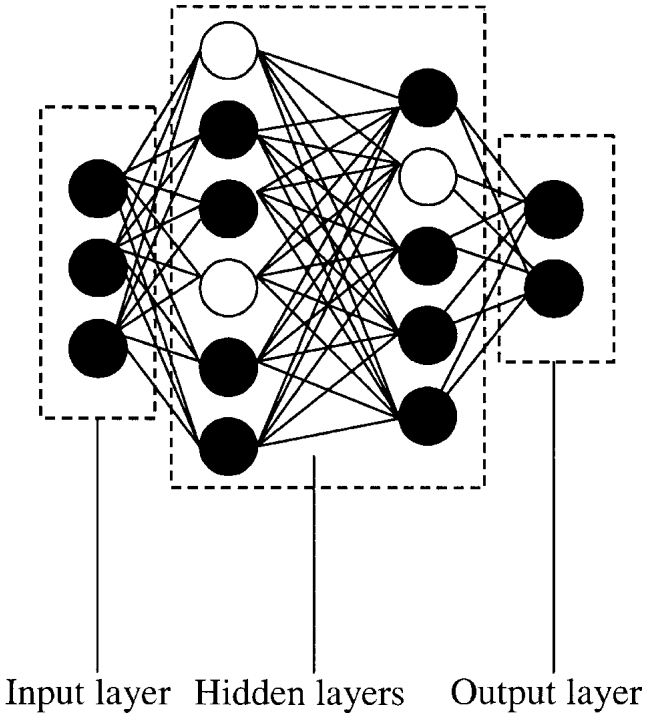

Fig. A1 A typical MLP (multilayer perceptron) showing the architecture of feed-forward structure. Neurons in white are enlarged in Fig. A2

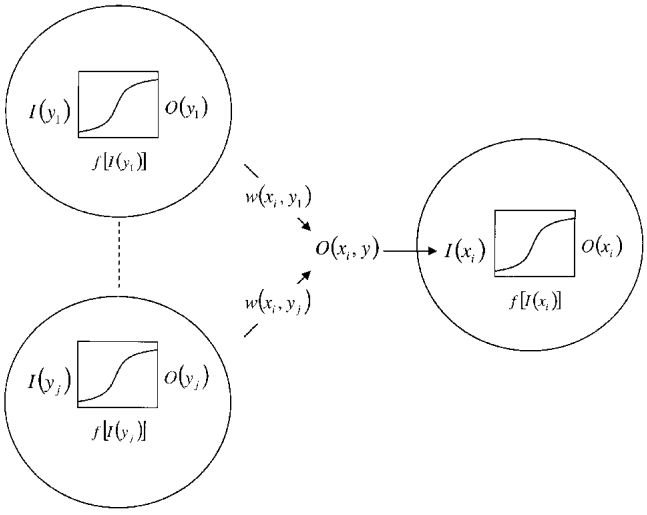

Fig. A2 Principle of connection in a feed forward network and the related quantities

$$I(x_i) = w(x_i,y_j)O(y_j) = O(x_i,y) \quad j = 1,N_y \tag{Eq A1}$$

where $w(x_i,y_i)$ is the weight between neuron x_i from the layer x and neuron y_j from the layer y and $O(y_i)$ is the output signal of neuron y_i from layer y.

The output signal of each processing parameter is then given by

$$O(x_i) = f[I(x_i)] \tag{Eq A2}$$

where $f[I(x_i)]$ is called the activation function (the transfer function) operating a nonlinear transformation on the input of neuron x_i from layer x. If the activation function depends on the neuron x_i, f becomes f_{xi}. This transformation is required because the sum of the output signals is linear, and this is not suitable to discover nonlinear correlations.

At the beginning of the training procedure, each weight is initialized to an arbitrary value. In the case of this study, this value was equal to 1. After propagating the output signal of each neuron until it reaches the output layer, the first output vector is obtained. It is compared with the real output given by the I/O example. For that purpose, an error function is calculated based on the quadratic error. It is firstly calculated at the output layer to tune the corresponding weights, and it is secondly back propagated to the internal layers to tune the other weights (Fig. A3). The magnitude and direction of the weight update is given, in this study, by the quick propagation algorithm.

A2. Quick Propagation Paradigm

This paradigm relies on the minimization of the quadratic error that can be written at the output layer, using Einstein notation:

$$E_z = \frac{1}{2}[r_k - O(z_k)]^2 \quad k = 1,N_z \tag{Eq A3}$$

where r_k is the correct output response at neuron k from the output layer z. $O(z_k)$ is the resulted output signal at neuron z_k from the output layer z and for the considered weight population.

Based on the error expression, the error gradient of the w_{jk} weight estimation is expressed then as:

$$\nabla E_z(y_j,z_k) = \frac{\partial E_z}{\partial w(y_j,z_k)} \tag{Eq A4}$$

where z_k and y_j relate to neurons in the z output layer and in the backward layer y, respectively.

Using the chain rule, Eq A4 can be rewritten as:

$$E\nabla E_z(y_j,z_k) = \frac{\partial E_z}{\partial I(z_k)} \times \frac{\partial I(z_k)}{\partial w(y_j,z_k)} \tag{Eq A5}$$

Replacing then Eq A1, A2, and A3 into A5 leads to:

$$\begin{aligned}\nabla E_z(y_j,z_k) &= f'[I(z_k)](r_k - O(z_k)) \times \frac{\partial[w(y_j,z_k)O(y_j)]}{\partial w(y_j,z_k)} \\ &= f'[I(z_k)](r_k - O(z_k)) \times O(y_j)\end{aligned} \tag{Eq A6}$$

where f' refers to the first derivative and $O(y_j)$ to the output signal at neuron j from layer y.

Now, this last expression can be calculated because all terms are known.

To compute the error gradient at a given internal connection, the same formulation holds to:

$$\nabla E_y(x_i,y_j) = \frac{\partial E_y}{\partial O(y_j)} \times \frac{\partial O(y_j)}{\partial I(y_j)} \times \frac{I(y_j)}{\partial w(x_i,y_j)} \tag{Eq A7}$$

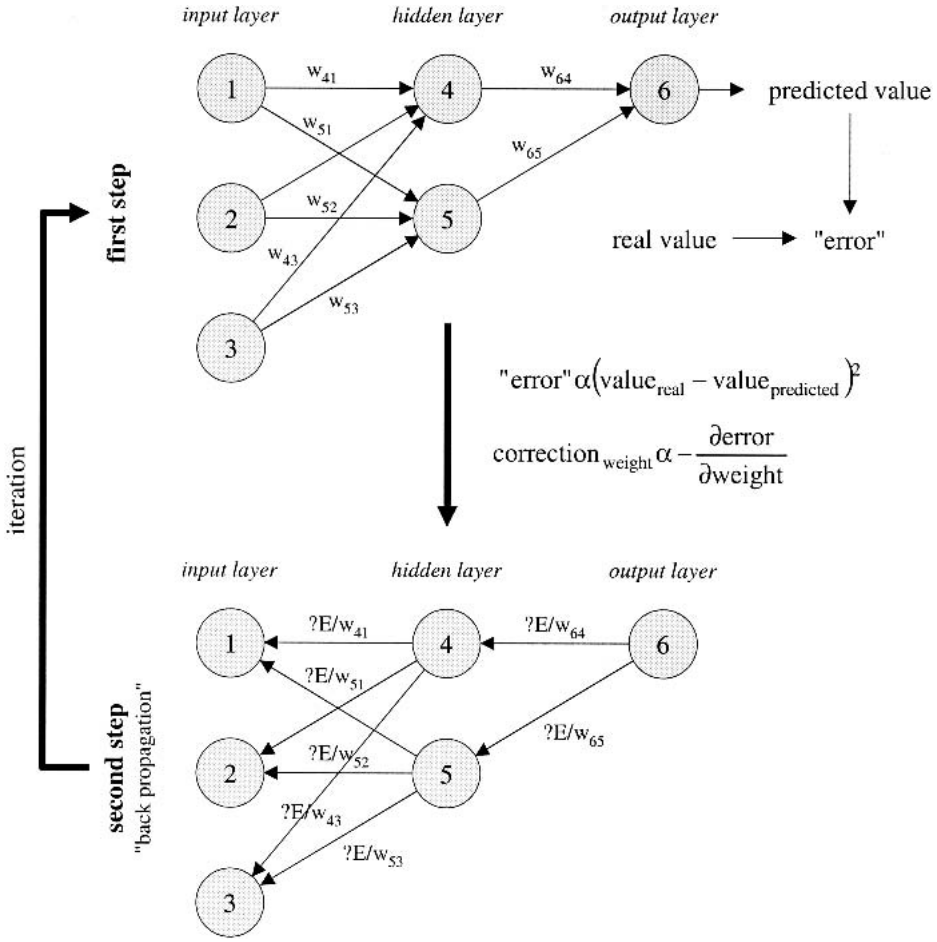

Fig. A3 Logic flow chart of the back propagation paradigm implemented to train an ANN

Considering the same expressions as Eq A1 and A2 for the layer y leads to:

$$\nabla E_y(x_i,y_j) = \frac{\partial E_y}{\partial O(y_j)} \times f'[I(y_j)] \times O(x_i) \qquad \text{(Eq A8)}$$

The last partial derivative of Eq A8 can be expressed as:

$$\frac{\partial E_y}{\partial O(y_j)} = \frac{\partial E_y}{\partial I(z_k)} \times \frac{\partial I(z_k)}{\partial O(y_j)} \quad k = 1,N_z \qquad \text{(Eq A9)}$$

Introducing into Eq A9 the weight population between layer y and layer z leads to:

$$\frac{\partial E_y}{\partial O(y_j)} = \frac{\partial E_y}{\partial I(z_k)} \times \frac{\partial [w(y_j,z_k)O(y_j)]}{\partial O(y_i)} = \frac{\partial E_z}{\partial I(z_k)} \times w(y_j,z_k) \quad k = 1,N_z \qquad \text{(Eq A10)}$$

Replacing the derivative term by its expression Eq A6 leads to:

$$\frac{\partial E_y}{\partial O(y_j)} = f'[I(z_k)](r_k - O(z_k)) \times w(y_j,z_k) \quad k = 1,N_z \qquad \text{(Eq A11)}$$

Thus,

$$\nabla E_y(x_i,y_j) = f'[I(z_k)](r_k - O(z_k)) \times w(y_j,z_k) \times f'[I(y_j)] \times O(x_i) \quad k = 1,N_z \qquad \text{(Eq A12)}$$

This last equation expresses the error gradient between the neuron x_i from layer x and the neuron y_j from layer y as function of the error at the output layer k.

As the error gradient at any connection is known giving the difference $r_k - O(z_k)$ at the output layer the weight update can be performed. In the case of the quick propagation paradigm, it is given as:

$$\Delta w(x_i,y_j)^t = \frac{\nabla E_y(x_i,y_j)^t}{\nabla E_y(x_i,y_j)^{t-1} - \nabla E_y(x_i,y_j)^t} \times \Delta w(x_i,y_j)^{t-1} \qquad \text{(Eq A13)}$$

where the superscript t refers to the epoch.

It can be seen from Eq A13 that the weight modification relies on the approximation of the error E. In fact, the quick propagation paradigm adapts the acceleration and the direction of the weight modification to minimize the time needed to find an optimal weight set. This is why it is considered faster than the standard back propagation supervised learning.

References

1. C. Moreau, Towards a Better Control of Thermal Spray Process, *Thermal Spray: Meetings the Challenge of the 21st Century,* C. Coddet, Ed., ASM International, 1998, pp 1681-1693
2. A. Refke, G. Barbezat, and M. Loch, The Benefit of an On-line Diagnostic System for the Optimization of Plasma Spray Devices and Parameters, *New Surfaces for a New Millennium,* C.C. Berndt, K.A. Khor, and E.F. Lugscheider, Ed., ASM International, 2001, pp 765-770
3. C. Moreau, P. Gougeon, M. Lamontagne, V. Lacasse, G. Vaudreuil, and P. Cielo, On-line Control of the Plasma Spraying Process by Monitoring the Temperature, Velocity and Trajectory of In-flight Particles, *Thermal Spray Industrial Applications,* C.C Berndt and S. Sampath, Ed., ASM International, 1994, pp 431-437
4. M. Friis and C. Persson, Process Window for Plasma Processes, *New Surfaces for a New Millennium,* C.C. Berndt, K.A. Khor, and E.F. Lugscheider, Ed., ASM International, 2001, pp 1313-1319
5. J.M. Guilemany, J. Nin, J. Delgado, and C. Lorenzana, On-Line-Monitoring of Stainless Steel Coatings Obtained by APS Processes, *Conference Proceedings of ITSC 2002,* E. Lugscheider, Ed., DVS-Verlag Düsseldorf, Germany, 2002, pp 86-90
6. P. Nylén, J. Wigren, J. Idetjärn, and L. Pejryd, On-Line Microstructure and Property Control of Thermal Sprayed Abrasive Coatings, *New Surfaces for a New Millennium,* C.C. Berndt, K.A. Khor, and E.F. Lugscheider, Ed., ASM International, 2001, pp 1213-1220
7. P. Fauchais and M. Vardelle, Plasma Spray Processes: Diagnostics and Control, *Pure Appl. Chem.,* 1999, Vol 71, pp 1909-1918
8. L. Leblanc and C. Moreau, Long-Term Stability of Plasma Spraying, *J. Therm. Spray Technol.,* 2002, Vol 11, pp 380-386
9. J.F. Bisson, B. Gauthier, and C. Moreau, Effect of Plasma Fluctuations on In-flight Particle Parameters – Part II, *Conference Proceedings of ITSC 2002,* E. Lugscheider, Ed., DVS-Verlag, Düsseldorf, Germany, 2002, pp 666-671, pp 86-90
10. J-E. Döring, R. Vassen, and D. Stöver, The Influence of Spray Parameters on Particle Properties, *Conference Proceedings of ITSC 2002,* E. Lugscheider, Ed., DVS-Verlag, Düsseldorf, Germany, 2002, pp 440-445
11. J.R. Fincke, W.D. Swank, R.L. Bewley, D.C. Haggard, M. Gevelber and D. Wroblewski, Diagnostic and Control in the Thermal Spray Process, *Surf. Coat. Technol.,* 2001, Vol 146-147, pp 537-543
12. Fr.-W. Bach, R. Hennne, V. Borch, K. Landes, T. Streibl, E. Lugscheider, A. Fischer, K. Seemann, T. Copitzky, and J. Prehm, Process Diagnostics at Thermal Spraying Processes—New Experiments from Current Projects of the DFG-Sponsored Research Group, *Conference Proceedings of ITSC 2002,* E. Lugscheider, Ed., DVS-Verlag, Düsseldorf, Germany, 2002, pp 78-90
13. T.J. Zappia, D. Harvey, C. Madden, and A. Matteson, Fuzzy Logic and Spray Forming Process, Proceedings SPIE Vol. 2061, *Applications of Fuzzy Logic Technology,* B. Bosacchi and J.C. Bezdek, Ed., SPIE, Bellingham, WA, 1993, pp 504-515
14. C.J. Einerson, D.E. Clarck, B.A. Detering, and P.L. Taylor, Intelligent Control Strategies for the Plasma Spray Process, *Thermal Spray Coatings: Research, Design and Applications,* C.C. Berndt and T.F. Bernecki, Ed., ASM International, 1993, pp 205-211
15. D.E. Rumelhart, G.E. Hinton, and R.J. Williams, Learning Representations by Back Propagating Errors, *Nature,* 1986,Vol 323, pp 533-536
16. P.J. Werbos, Generalization of Back Propagation with Application to Recurrent Gas Market Model, *Neural Networks,* 1988, Vol 1, pp 339-356
17. S.E. Fahlman, Fast Learning Variations on Back Propagation: An Empirical Study, *Proceedings of the 1988 Connectionist Models Summer School,* D. Touretzky, G. Hinton, and T. Sejnowski, Ed., M. Kaufmann, San Mateo, CA, 1988, pp 38-51
18. J. Wigren and K. Täng, Some Considerations for the Routine Testing of Thermal Sprayed Coatings, *New Surfaces for a New Millennium,* C.C. Berndt, K.A. Khor, and E.F. Lugscheider, Ed., ASM International, 2001, pp 1221-1227
19. C. Bossoutrot, F. Braillard, T. Renault, M. Vardelle, and P. Fauchais, Preliminary Studies of a Closed Loop for a Feedback Control of Air Plasma Spray Processes, *Conference Proceedings of ITSC 2002,* E. Lugscheider, Ed., DVS-Verlag, Düsseldorf, Germany, 2002, pp 56-61
20. S. Kundas and A. Iiyuschenko, Computer Simulation of Plasma Spraying Processes, *New Surfaces for a New Millennium,* C.C. Berndt, K.A. Khor, and E.F. Lugscheider, Ed., ASM International, 2001, pp 925-932
21. L. Leblanc, P. Gougeon, and C. Moreau, Investigation of the Long-Term Stability of Plasma Spraying by Monitoring Characteristics of the Sprayed Particles, *Thermal Spray: A United Forum for Scientific and Technological Advances,* C.C. Berndt, Ed., ASM International, 1997, pp 567-575
22. I.A. Fisher, Variables Influencing the Characteristics of Plasma-Sprayed Coatings, *Int. Metall. Rev.,* 1972, Vol 17, pp 117-125
23. E. Pfender, Fundamental Studies Associated with the Plasma Spray Process, *Surf. Coat. Technol.,* 1988, Vol 34 (No. 1), pp 1-14
24. R.H. Henne, E. Bouyer, V. Borck, and G. Schiller, Influence of Anode Nozzle and External Torch Contour on the Quality of the Atmospheric DC Plasma Spray Process, *New Surfaces for a New Millennium,* C.C. Berndt, K.A. Khor, and E.F. Lugscheider, Z Ed., ASM International, 2001, pp 471-478
25. T. Elsken, Even on Finite Test Sets Smaller Nets May Perform Better, *Neural Networks,* 1999, Vol 10, pp. 369-385
26. L.P. Bartlett, For Valid Generalization the Size of the Weights is More Important Than the Size of the Network, *Advances in Neural Information Processing Systems 9,* M.C. Mozer, M.I. Jordan, and T. Petsche, Ed., The MIT Press, 1997, pp 134-140
27. M.M. Nelson and W.T. Illingworth, *A Practical Guide to Neural Nets,* 3rd ed., Addison-Wesley, 1991
28. S. Guessasma, G. Montavon, P. Gougeon, and C. Coddet, On the Neural Network Concept to Describe the Thermal Spray Deposition Process: Correlation Between In-flight Particles Characteristics and Processing Parameters *Conference Proceedings of ITSC 2002,* E. Lugscheider, Ed., DVS-Verlag, Düsseldorf, Germany, 2002, pp 483-488
29. P. Nylén, R. Bolot, A. Hansbo, and C. Coddet, Modeling and Measurement of Particle In-flight Characteristics of Atmospheric Plasma Sprayed Yttria Stabilized Zirconia *Heat and Mass Transfer Under Plasma Conditions 891,* Annals of the New York Academy of Sciences, P. Fauchais, J. van der Mullen, and J. Heberlein, Ed., New York Academy of Sciences, 1999, pp 236-245
30. K. Seemann, A. Fisher, and E. Lugscheider, Influence of Noise Factors at Atmospheric Plasma Spraying *Conference Proceedings of ITSC 2002,* E. Lugscheider, Ed., DVS-Verlag, Düsseldorf, Germany, 2002, pp 1007-1010
31. M. Prystay, P. Gougeon, and C. Moreau, Structure of Plasma Sprayed Zircona Coatings Tailored by Controlling the Temperature and Velocity of the Sprayed Particles, *J. Therm. Spray. Technol.,* 2001, Vol 10, pp 67-75
32. M. Friis, C. Persson, and J. Wigren, Influence of Particle In-Flight Characteristics on the Microstructure of Atmospheric Plasma Sprayed Yttria Stabilized ZrO_2, *Surf. Coat. Technol.,* 2001, Vol 141, pp 115-127
33. B. Pateyron, G. Delluc, M.F. Elchinger, and P. Fauchais, Thermodynamic and Transport Properties of Ar-H_2 and Ar-He Plasma Gases Used for Spraying at Atmospheric Pressure—Part 1. Properties of the Mixtures, *Plasma Chem. Plasma Process.,* 1992, Vol 12 (No. 4), pp 421-448
34. M. Boulos, P. Fauchais, E. Pfender, and M. Vardelle, Fundamentals of Plasma Particle Momentum and Heat Transfer in Thermal Spraying *Plasma Spraying: Theory and Applications,* R Suryanarayanan, Ed., World Scientific, Singapore, 1993, pp 17-42
35. P. Saravanan, V. Selvarajan, M.P. Srivastava, D.S. Rao, S.V. Joshi, and G. Sundararajan, Study of Plasma- and Detonation Gun-Sprayed Alumina Coatings Using Taguchi Experimental Design, *J. Therm. Spray Technol.,* 2000, Vol 9, pp 505-512
36. J.R. Mawdsley, Y.J. Su, K.T. Faber, and T.F. Bernecki, Optimization of Small-Particle Plasma-Sprayed Alumina Coatings Using Design Experiments, *Mater. Sci. Eng.,* 2001, Vol A380, pp 189-199